Mixed Conduction Mode Control for Inductor Minimization in Grid-Tied Inverter

Hoai Nam Le, Jun-ichi Itoh
Nagaoka University of Technology
1603-1 Kamitomioka Town
Nagaoka City, Niigata Prefecture, Japan
Tel.: +81 / (258) – 47.9533.
E-Mail: lehoainam@stn.nagaokaut.ac.jp
URL: http://itohserver01.nagaokaut.ac.jp/itohlab/index.html

***Abstract*— This paper proposes a mixed-conduction-mode (MCM) current control for a grid-tied inverter operating in both continuous current mode (CCM) and discontinuous current mode (DCM) in order to minimize an interconnected inductor. In general, a low interconnected inductor value worsens disturbance suppression of current controller, and leads to an increase in grid current total harmonic distortion (THD). In DCM, the disturbance-to-current transfer function becomes nonlinear and the disturbances such as the dead time voltage error are effectively suppressed. Therefore, the grid-tied inverter operating in MCM can achieve a low grid current THD. However, another DCM nonlinearity occurs in the duty-to-current transfer function, which makes control gain characteristic in DCM completely different from that in CCM. Therefore, the DCM nonlinearity compensation is proposed by using duty at previous calculation. The validity of the proposed current control is confirmed with a 1-kW 100-kHz prototype. Even when using the interconnected inductor with a normalized impedance of 0.16%, the grid current THD is reduced from 14.8% to 2.9% at rated load compared to the conventional CCM control. Furthermore, the inductor volume is reduced by 77.0%, whereas the converter loss is reduced by 36.5%.**

***Keywords*—Single-phase grid-tied inverter, Continuous current mode, Discontinuous current mode, Mixed conduction mode, Disturbance compensation.**

I. Introduction

IN recent years, researches on photovoltaic system (PV) has attracted many attentions due to the increasing demand of renewable resources [1]-[3]. H-bridge inverters are usually used in the PV system in order to convert DC power from solar panel into AC power in the conventional AC single-phase grid. In such grid-tied inverters, LCL filters are generally employed between the inverter and the grid in order to suppress current harmonics and meet grid current harmonic constraints as defined by standards such as IEEE-519-1992 [4]-[5]. This LCL filter, especially the interconnected inductor, accounts for a majority of the inverter volume [6]-[7]. By increasing switching frequency and reducing an inductor value, the interconnected inductor volume can be minimized. However, the grid-tied inverter generally operates in CCM, where the disturbance suppression performance worsens with the reduced inductor value. This leads to the increase in the grid current THD. In order to overcome this problem, a disturbance observer which is designed based on CCM transfer function is utilized. The disturbance observer can suppress the disturbance effects on the current control and allows the reduction of the inductor value. Nevertheless, this method requires high speed controllers such as, e.g. field-programmable gate array (FPGA), in order to estimate the rapidly-changing disturbances, e.g. the dead-time error voltage [8].

As another approach, the disturbance effects can be reduced by DCM. The zero-current interval in DCM introduces the nonlinearity into the disturbance-to-current transfer function, which effectively suppresses the disturbance effects such as the dead time voltage error. However, another nonlinearity occurs in the duty-to-current transfer function, which makes the current control gain in DCM completely different from that of CCM [9]-[10]. A nonlinearity compensation has been proposed and effectively achieves the current command response as same as CCM [10]. Nevertheless, the proposed DCM current controller can be applied only in DCM, which implies that the grid-tied inverter has to operate in DCM over entire load range. This design significantly increases conduction loss of switching devices due to high current ripple of DCM at rated load. Therefore, many control methods which allow the inverter to operate in both CCM and DCM have been proposed to improve the conversion efficiency [11]-[14]. However, these MCM control method becomes dependent on the inductor value, which decays the robustness of the controller against the change of the inductor value [15].

This paper proposes a novel MCM current control for the grid-tied inverter operating in both CCM and DCM. The DCM nonlinearity in the disturbance characteristic is used to reduce the grid current THD, whereas the DCM nonlinearity in the duty-to-current transfer function is compensated by using the duty at the previous calculation period. Meanwhile, the current mode determination between CCM and DCM is accomplished by comparing the DCM duty and the CCM duty at the output of the controller. Thank to this method, the current feedback control is independent of the inductor value and can operate at any load condition. This paper is organized as follows: first the problems with the increasing grid current THD when the inductor value is reduced in CCM operation is explained. Next, two DCM nonlinearities are investigated when the power factor is lower than one in order to stably operate the grid-tied inverter at any load condition. Then the MCM current control for both CCM and DCM is proposed in order to obtain the low grid current THD with the small inductor value. Finally, the effectiveness of the proposed current control is confirmed experimentally with a 1-kW prototype. The comparisons of the grid current THD and the conversion efficiency are demonstrated.

II. Proposed Mixed Conduction Mode Current Control

A. Current Distortion in Conventional Continuous Current Mode Control

Fig. 1 indicates the circuit configuration of the single-phase grid-tied inverter. In this paper, a single-phase H-bridge inverter is applied due to its simplicity. The LCL filter connects the inverter to the grid in order to suppress the current harmonics of the inverter output current i_{out}. Note that the grid has its own intrinsic inductor L_g, the value is different depending on the type and the condition of the grid.

Fig. 2 indicates the conventional CCM feedback current control block with a typical dead-time error voltage compensation. Note that the grid current i_g and the grid voltage v_g are assumed to be as same as i_{out} and the voltage v_{Cf} across the filter capacitor C_f, respectively, because the cutoff frequency of the LCL filter is designed to be much higher than the bandwidth of the current control loop. The amplitude of the disturbance-voltage-to-current transfer function in CCM which is also entitled the gain of the disturbance response $|G_{dis\_CCM}|$ is derived from Fig. 2 and expressed as in

$$|G_{dis\_CCM}| = \frac{1}{L\omega_n}\frac{1}{\sqrt{4\zeta^2 + \frac{\omega_n^2}{\omega^2}\left(1-\frac{\omega^2}{\omega_n^2}\right)^2}} \quad \text{.......(1)},$$

where L is the inverter-side inductor value, ω is the disturbance angular frequency, ω and ω_n are the damping factor and the angular frequency of the current controller, respectively.

Fig. 3 depicts the gain of the disturbance response in CCM under different conditions of L. Because $|G_{dis\_CCM}|$ is inversely proportional to L, the disturbance effects increase 10 times when L is reduced from 1 p.u. to 0.1 p.u.. Consequently, this worsens the disturbance response. In general, when the typical dead-time error voltage compensation is applied with the high L, the current distortion is effectively reduced. However, when L is greatly reduced, only a small mismatch between the estimated and actual dead-time error voltage ($v_{deadtime\_est}$ and $v_{deadtime}$) which is caused by such as the current detection delay, results in a high current distortion due to the greatly-increasing gain of the disturbance response $|G_{dis\_CCM}|$. Note that by increasing the angular frequency of the current controller ω_n, the gain of the disturbance response $|G_{dis\_CCM}|$ can be reduced, i.e. the current distortion can be reduced. However, a high bandwidth current control requires a high speed controller, which is an undesired solution.

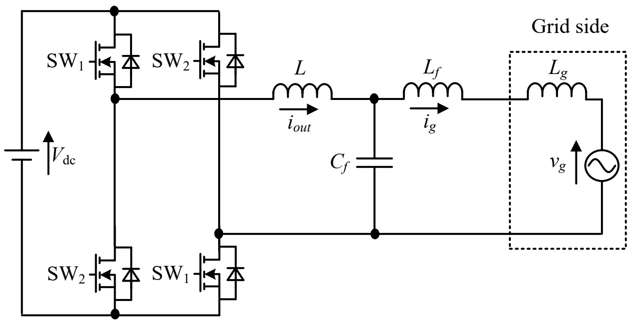

Fig. 1. Single-phase H-bridge grid-tied inverter with LCL filter. A single-phase H-bridge inverter is applied due to its simplicity, which is important for stability analysis and reliability design.

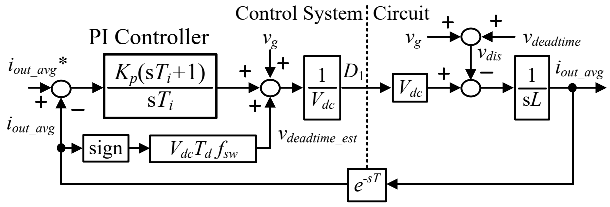

Fig. 2. Conventional CCM feedback current control block with typical dead-time error voltage compensation. When the interconnected inductor is minimized by reducing the inductor value, the inverter become more vulnerable to the disturbances, i.e. the increase in the disturbance gain.

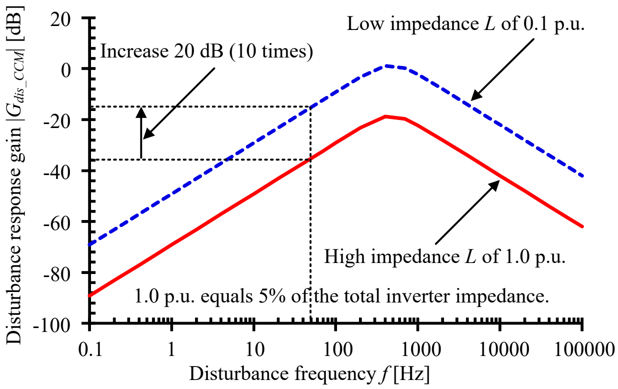

Fig. 3. Disturbance response gain in CCM. The minimization of the inductors in CCM is limited by the increase in the disturbance gain.

B. Compensation of Discontinuous-Current-Mode Nonlinearity in Duty-To-Current Transfer Function

Fig. 4 indicates the grid-tied inverter operation under different conditions of the power factor. Fig. 4(a), (b) shows the relationship between the grid voltage v_g and the output current i_{out} of the inverter at the unity power factor and the power factor below one, respectively. Meanwhile, Fig. 4(c), (d) depicts the inverter operation mode and the output current waveform when the inverter operates in powering mode at interval *ii* in Fig. 4(b) and generation mode at interval *i* in Fig. 4(b), respectively. Note that the grid-tied inverter is operated in bipolar modulation in order to reduce common current, whereas the grid-side inductors L_g, L_f, and the filter capacitor C_f are omitted due to the simplification. As shown in Fig. 4(a), the inverter operates in only the powering mode when the power factor is unity. On the other hand, the in-

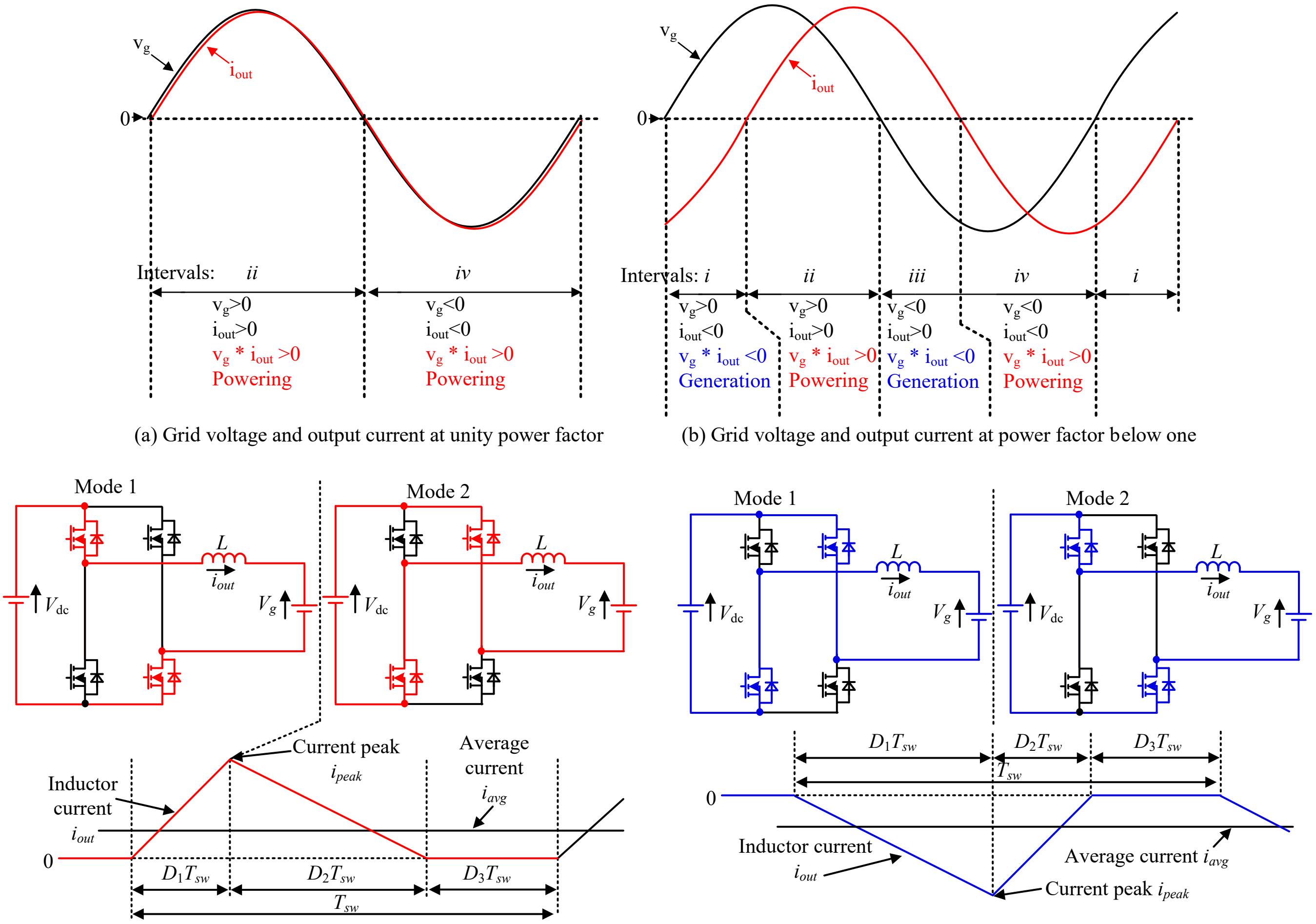

(a) Grid voltage and output current at unity power factor

(b) Grid voltage and output current at power factor below one

(c) Inverter operation mode and output current waveform in powering mode (cf. interval *ii* of Fig. 4(b))

(d) Inverter operation mode and output current waveform in generation mode (cf. interval *i* of Fig. 4(b))

Fig. 4. Grid-tied inverter operation under different conditions of power factor. Different from the CCM operation, the inverter operation mode in DCM depends on the relationship between the grid voltage v_g and the output current i_{out} of the inverter, i.e. the powering mode or the generation mode. This is because the zero-current interval introduces nonlinearities into the DCM operation.

verter alternatively operates in the powering mode and the generation mode when the power factor is below one as shown in Fig. 4(b). Consequently, as shown in Fig. 4(c), (d), the applying order of mode 1 and mode 2 in the powering mode is flipped compared to that in the generation mode. The reason is that different from the CCM operation, the inverter operation mode in DCM depends on the relationship between the grid voltage v_g and the output current i_{out} of the inverter, i.e. the powering mode or the generation mode. Therefore, in order to control the grid-tied inverter in DCM, the circuit model has to be analyzed in each the powering mode and the generation mode. For the sake of brevity, only the operation in the powering mode is discussed in the following. However, the operation in the generation mode is derived analogously.

Considering the inverter operation and the output current waveform in the power mode shown in Fig. 4(c) (cf. the interval *ii* in Fig. 4(b)), D_1, D_2 and D_3 denote the duties of the first, the second and the zero-current interval. The equation based on the average model of the inverter shown in Fig. 4(c) is given by (2) [9]-[10],

$$V_L = D_1(V_{dc} - V_g) - D_2(V_{dc} + V_g) \quad (2)$$

where V_L is the average inductor voltage, V_{dc} is the DC-link voltage and V_g is the grid voltage. The average current i_{avg} and the current peak i_{peak}, which are shown in Fig. 4(c) are expressed as,

$$i_{avg} = \frac{i_{peak}}{2}(D_1 + D_2) \quad (3)$$

$$i_{peak} = \frac{V_{dc} - V_g}{L} D_1 T_{sw} \quad (4)$$

where T_{sw} is the switching period. Substituting (4) into (3) and solving the equation for the duty D_2. The duty D_2 is expressed by

$$D_2 = \frac{2Li_{avg}}{D_1 T_{sw}(V_{dc} - V_{ac})} - D_1 \quad (5),$$

Substituting (5) into (2) in order to remove the duty D_2 and represent (2) as a function of only the duty D_1, then (6) is obtained.

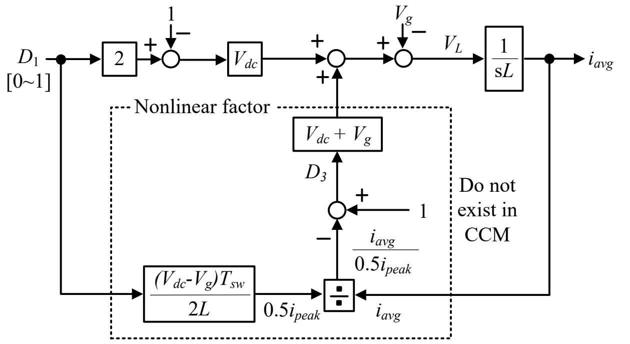

Fig. 5. Circuit model of inverter operated in DCM at powering mode. In DCM, the current control depends greatly on the current value, i.e. the nonlinearities occurring in the duty-ratio-to-current transfer function and the disturbance-to-current transfer function.

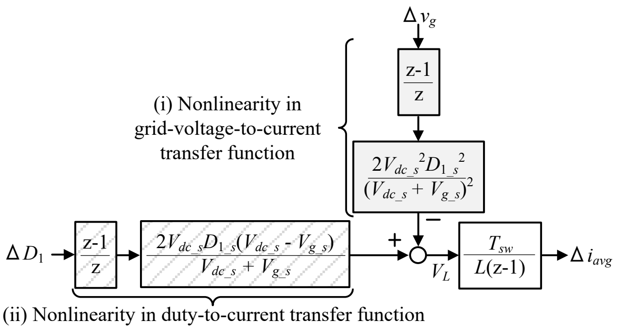

Fig. 6. Discretized circuit model in DCM at powering mode. The original idea of the DCM nonlinearity compensation is to estimate the duty at steady states by the duty at the previous calculation. Consequently, the inductor value is not required in the DCM nonlinearity compensation.

$$V_L = V_{dc}(2D_1 - 1) - V_g + (V_{dc} + V_g)\left\{1 - \frac{2Li_{avg}}{(V_{dc} - V_g)D_1T_{sw}}\right\} \qquad (6)$$

Then, the inverter model in DCM is established based on (6).

Fig. 5 illustrates the circuit model of the inverter operating in DCM at powering mode which is based on (6). In CCM, the dash line part does not exist, because the average current i_{avg} equals to the half current peak $i_{peak}/2$. On the other words, this makes the zero-current interval D_3T_{sw} shown in Fig. 3 become zero. However, in DCM, the zero-current interval introduces the nonlinearities into the DCM transfer function. The design of the compensation part for the DCM nonlinearity is explained as in [10]. The circuit model in Fig. 5 is linearized and discretized at steady state points.

Fig. 6 depicts the discretized circuit model at powering mode. Note that V_{dc_s}, V_{g_s}, and D_{1_s} are the DC-link voltage, the grid voltage and the duty at steady state points, whereas Δv_g, ΔD_1, and Δi_{avg} are the small signals of the grid voltage, the duty and the average current, respectively. The zero-current interval introduces nonlinearities in the grid-voltage-to-current transfer function and the duty-to-current transfer function.

Fig. 7 (a)-(c) indicates the proposed DCM current controls for the powering mode, for the generation mode and for any conditions of the power factor, respectively. As shown in Fig. 7(a), in order to compensate the DCM nonlinearities at the output of the PI controller designed in CCM, the nonlinearity in the duty-to-current transfer function in Fig. 6 is set as 1, whereas the nonlinearity in the grid-voltage-to-current transfer function is eliminated by feeding forward the grid voltage to the output of the PI controller. In principle, the current control in Fig. 7(b) is the same as that in Fig. 7(a). However, the sign of the absolute value of the grid voltage in Fig. 7(b) is opposite to that in Fig. 7(a), because as shown in Fig. 5(c), (d), the applying order of mode 1 and mode 2 in the powering mode is flipped compared to that in the generation mode. In order to control the DCM current under any conditions of the power factor, the combination of the current control from Fig. 7(a) and (b) is required. By using the information of the output current polarity, the proposed DCM nonlinearity compensation can be employed over entire range of the power factor.

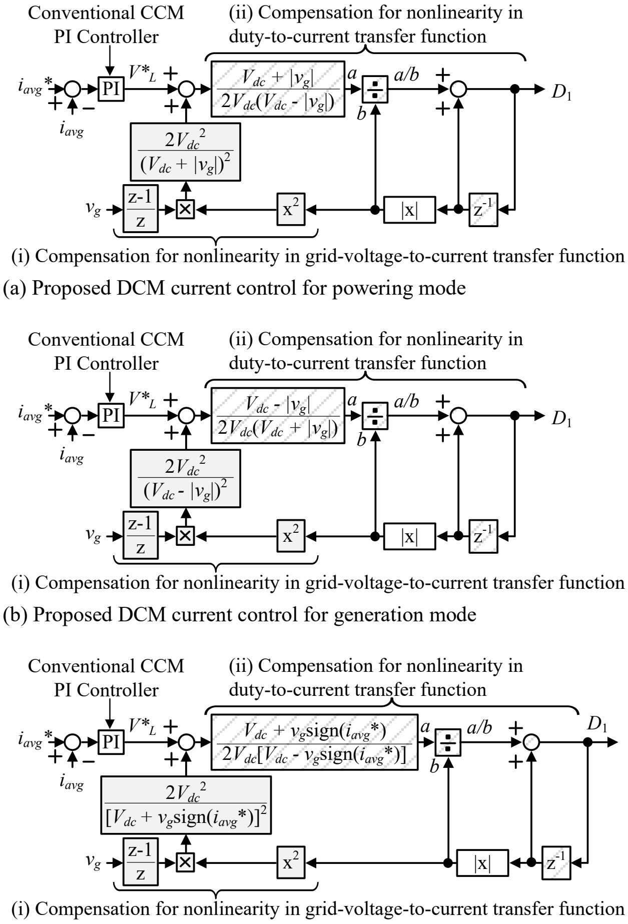

(a) Proposed DCM current control for powering mode

(b) Proposed DCM current control for generation mode

(c) Proposed DCM current control for any condition of power factor

Fig. 7. Proposed DCM current control for any conditions of power factor. By using the information of the output current polarity, the proposed DCM nonlinearity compensation can be employed over entire range of the power factor.

Fig. 8 shows the gain of the disturbance response in CCM and DCM under different conditions of the steady-state duty-ratio D_{1_s}. In CCM, the minimization of the inductor value L worsens the disturbance response. On the other hand, in DCM when the steady-state duty-ratio D_{1_s} becomes smaller, the disturbance response gain in DCM decreases. The reason is that the proposed DCM nonlinearity compensation for the current command response does not compensate for the DCM nonlinearity in the disturbance response. Consequently, the disturbance response depends on the steady-state duty-ratio D_{1_s}. Therefore, by utilizing this nonlinearity characteristic in which the disturbance gain decreases greatly with the small steady-state duty-ratio D_{1_s}, i.e. the interval near the current zero-crossing point or the light load, the current distortion can be reduced.

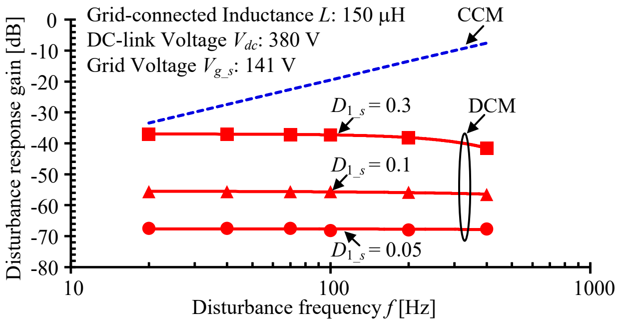

Fig. 8. Disturbance characteristics in CCM and DCM. The DCM nonlinearity in the disturbance-to-current transfer function makes the DCM current more resistant to the disturbance than the CCM current. Therefore, the interconnected inductor can be further minimized in DCM.

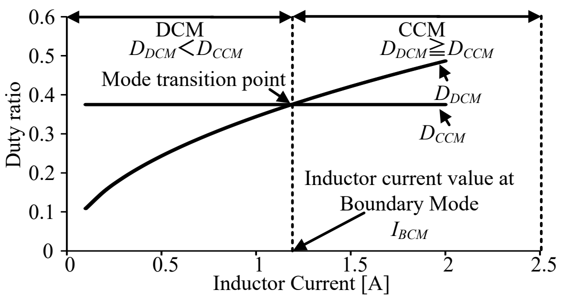

Fig. 9. Relationship among CCM duty, DCM duty and current mode. When the circuit operates in DCM, the DCM duty becomes smaller than the CCM duty and vice versa. Using this relationship, the current mode determination is achieved without using the inductor value.

C. Current Mode Determination

Fig. 9 shows the relationship among the CCM duty, the DCM duty and the current mode. In conventional current mode determination, the average current (the detection value i_{avg} or the command value i_{avg}*) is compared with the current value I_{BCM} at the boundary between CCM and DCM, which is calculated by using the inductor value. Consequently, when the actual inductor value is different from the nominal value, the current mode cannot be accurately determined by the conventional method. On the other hand, the proposed current mode determination focuses on the relationship between the CCM duty and the DCM duty when the current mode alternates. In particular, when the circuit operates in DCM, the DCM duty becomes smaller than the CCM duty and vice versa. Therefore, using this relationship, the proposed current mode determination is achieved without using the inductor value. This makes the MCM controller robust against the change of the inductor value.

Fig. 10 indicates the proposed MCM current control and the waveform of the current mode alternation. The CCM duty $Duty_{CCM}$ is calculated without using the inductor value. Similarly, the inductor value is unnecessary in the calculation of the DCM duty $Duty_{DCM}$, because the inductor value is not used in the DCM nonlinearity compensation. Consequently, the relationship between the CCM duty and the DCM duty which is independent from the inductor value is achieved. Thank to this, the proposed MCM current control can be applied even when the inductors with high tolerance are used.

III. Laboratory Setup

Table I depicts the experimental parameters. The operation frequency of the current controller is synchronized with the sampling frequency of 20 kHz despite of the high switching frequency of 100 kHz, which enables the use of low speed controllers.

Fig. 11 depicts the prototypes of the inverter-side inductors L under different conditions of the inductor impedance $\%Z_L$ normalized by the based impedance. Ferrite is chosen

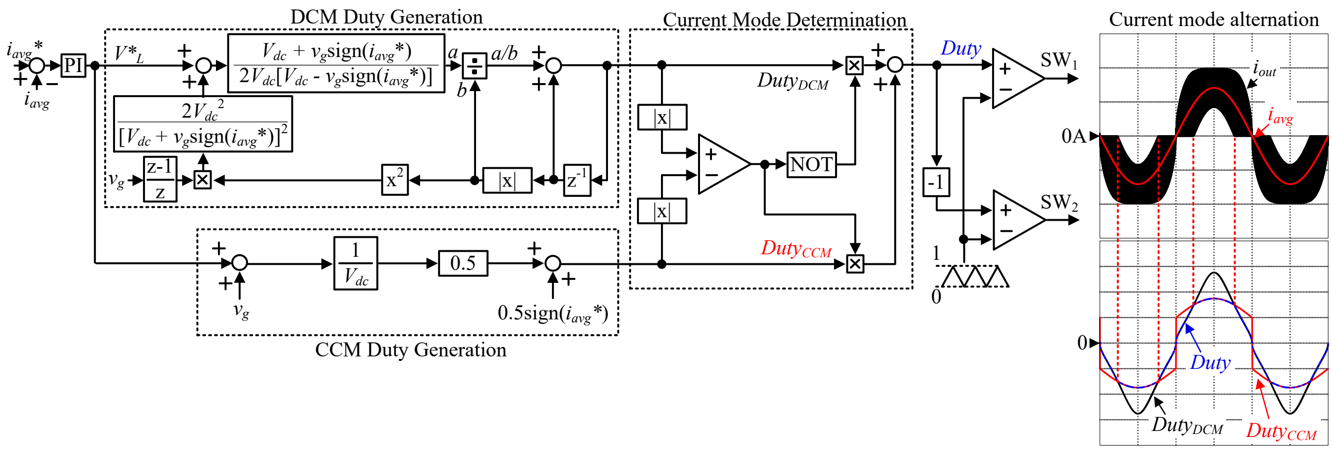

Fig. 10. Proposed MCM current control for grid-tied inverter operating under any condition of power factor. The proposed MCM current control is independent from the inductor value because the inductor value is not used in both the DCM nonlinearity compensation and the current mode determination.

TABLE I
SYSTEM PARAMETERS.

Circuit Parameter		
V_{DC}	DC link Voltage	380 V
v_g	Grid Voltage	200 Vrms
P_n	Nominal Power	1 kW
Switching Device (SiC MOSFET)		SCH2080KE
Core material and Litz wire		Ferrite N87, 100/ϕ0.1
f_g	Grid Frequency	50 Hz
Z_b	Base Impedance	40 Ω
C_b	Base Capacitance	79.6 μF
C_f	Filter Capacitor	0.5 μF
f_{sw}	Switching Frequency	100 kHz
Current Controller Parameter		
f_{samp}	Sampling Frequency	20 kHz
ζ	Damping Factor	1.4
f_c	Cutoff Frequency	1 kHz

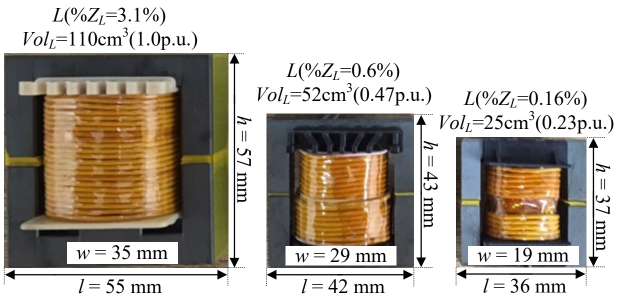

Fig. 11. Prototypes of inverter-side inductors under different conditions of inductor impedance normalized by base impedance. By reducing the impedance of the inverter-side inductor $\%Z_L$ from 3.1% to 0.16%, the inductor volume is reduced by 77%.

to be the core material in order to minimize the core loss at the switching frequency of 100 kHz, whereas Litz wire is used in order to minimize the winding loss coming from the proximity effect and the skin effect. By the application of DCM, the normalize impedance of the inductor impedance $\%Z_L$ can be minimized without worsening the disturbance response as shown in Fig. 8. Consequently, by reducing the impedance of the inverter-side inductor $\%Z_L$ from 3.1% to 0.16%, the inductor volume is reduced by 77%.

Fig. 12 and Fig. 13 shows the grid voltage, the grid current and the inverter output current of the conventional CCM current control and the proposed MCM current control at rated load of 1kW and at light load of 200W, respectively. The IEEE-519-1992 standards require the grid current THD below 5% at rated load, which can be accomplished simply with the high impedance of the inverter-side inductor $\%Z_L$ as shown in Fig. 12 (a). However, as L is reduced to minimize the interconnected inductor, the disturbance effects in CCM increase with small $\%Z_L$ as shown in Fig. 3. Consequently, the grid current THD increases from 1.5% to 14.8% when $\%Z_L$ is reduced from 3.1% to 0.16%. This problem can be overcome by increasing the control bandwidth of the current controller, which is difficult to employ with low speed microprocessors. On the other hand, when the inverter is operated in MCM, the disturbance effects naturally reduce at low duties as shown in Fig. 8, i.e. the zero-crossing intervals,

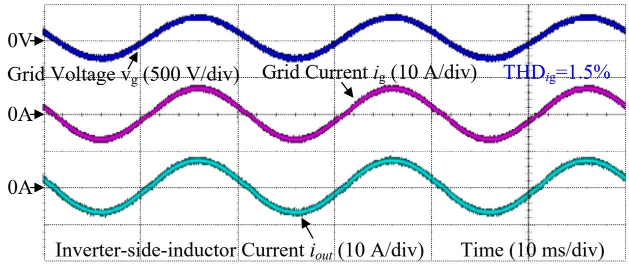

(a) Conventional CCM current control with $\%Z_L$ = 3.1% at rated load

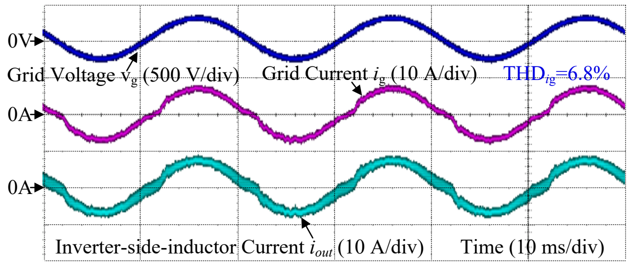

(b) Conventional CCM current control with $\%Z_L$ = 0.6% at rated load

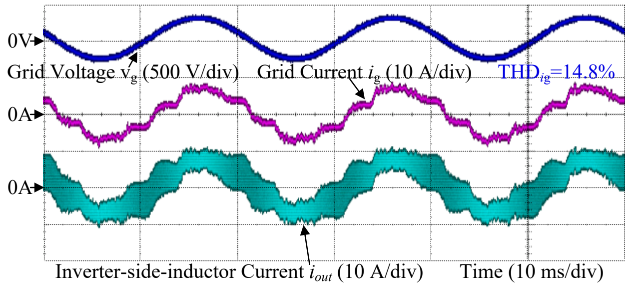

(c) Conventional CCM current control with $\%Z_L$ = 0.16% at rated load

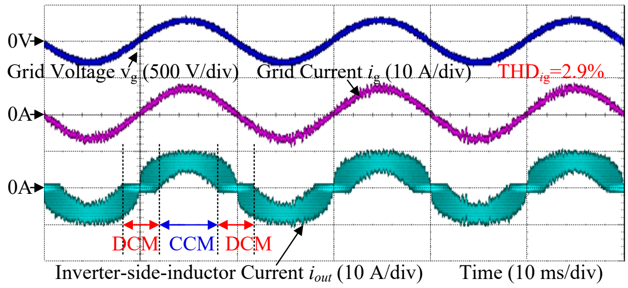

(d) Proposed MCM current control with $\%Z_L$ = 0.16% at rated load

Fig. 12. Grid voltage, grid current and inverter output current of conventional CCM current control and proposed MCM current control at rated load of 1kW. When the inverter is operated in MCM, the disturbance effects naturally reduce at low duties, i.e. the zero-crossing intervals, due to the nonlinearity in the disturbance response.

due to the nonlinearity in the disturbance response. Therefore, the low grid-current THD of 2.9% is achieved with the proposed MCM current control even when $\%Z_L$ is reduced to 0.16%. Similarly, the grid current THD at light load of 200W is also reduced from 27.6% to 2.5%.

Fig. 14 shows the comparison of the grid current THD and the conversion efficiency between the conventional CCM current control and the proposed MCM current control with different of normalized impedances. Even when the normalized impedance of the grid-side inductor $\%Z_L$ is min-

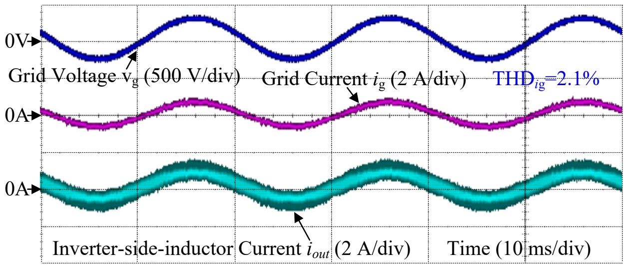

(a) Conventional CCM current control with $\%Z_L$ = 3.1% at light load

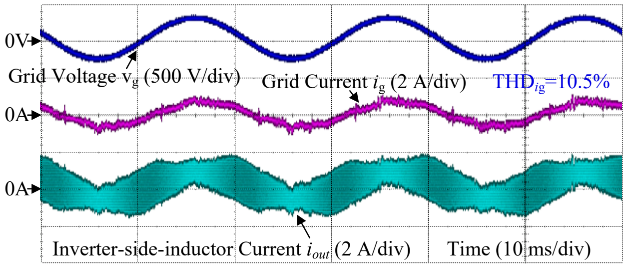

(b) Conventional CCM current control with $\%Z_L$ = 0.6% at light load

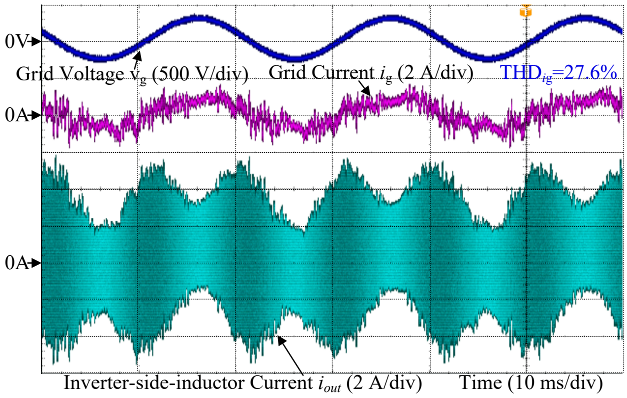

(c) Conventional CCM current control with $\%Z_L$ = 0.16% at light load

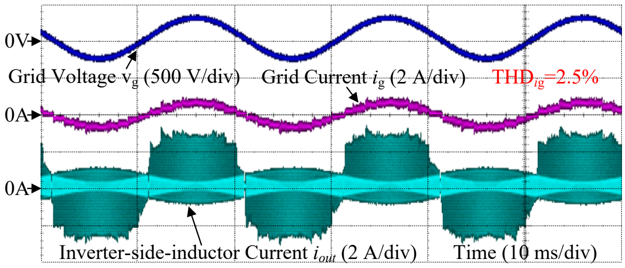

(d) Proposed MCM current control with $\%Z_L$ = 0.16% at light load

Fig. 13. Grid voltage, grid current and inverter output current of conventional CCM current control and proposed MCM current control at light load of 200W.

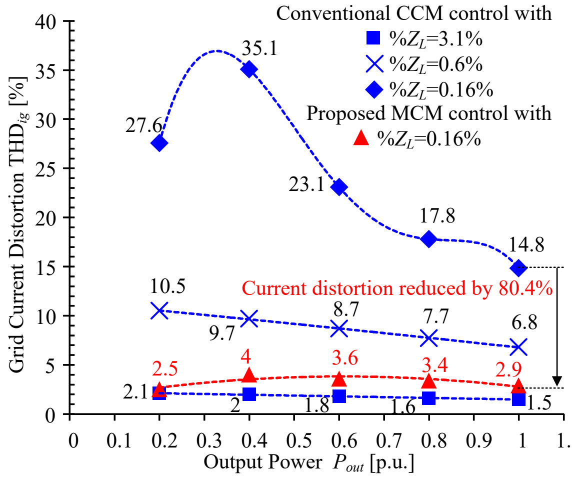

(a) Grid current THD characteristics

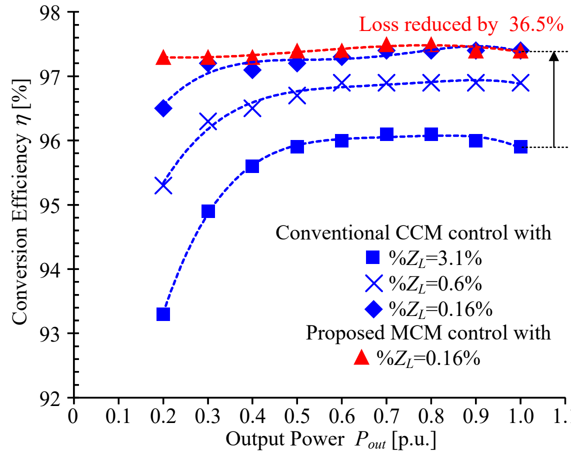

(b) Conversion efficiency characteristics

Fig. 14. Comparison of grid current THD and conversion efficiency between conventional CCM current control and proposed MCM current control with different of normalized impedances. The trade-off relationship between the grid current THD and the efficiency occurs in the conventional CCM current control, whereas the proposed MCM control can achieve both the low grid current THD and the high efficiency.

imized to 0.16% of the inverter total impedance, the grid current THD is maintained to be lower than 5% over entire load range by applying the proposed MCM current control. Furthermore, by minimizing $\%Z_L$ to 0.16%, the efficiency is improved by 1.5% compared with the normalized impedance of $\%Z_L$=3.1%. Furthermore, in the conventional CCM current control, the lower the grid THD becomes, the higher the conversion loss becomes. On the other words, the trade-off relationship between the grid current THD and the efficiency occurs in the conventional CCM current control, whereas the proposed MCM control can achieve both the low grid current THD and the high efficiency.

Fig. 15 depicts the proposed MCM current control operation at the rated current and under different power factors. The low grid current THD can still be achieved at low power factor with the proposed MCM current control. On the other words, the proposed MCM current control provides the grid-tied inverter the capability of fault-ride-through. The effectiveness of the proposed MCM current control is confirmed by these experimental results.

IV. Conclusion

When the grid-connected inductor is minimized by reducing the inductor impedance, the disturbance effects increases highly in the CCM operation, which distorts the grid current. On the other hand, in the DCM operation, the non-

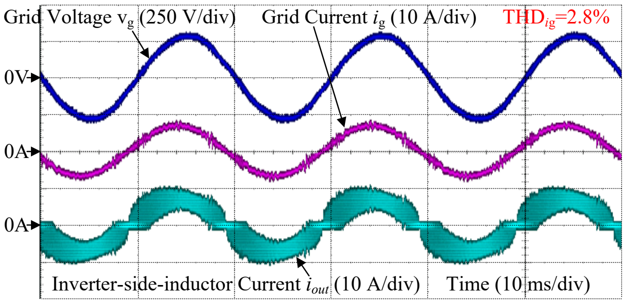

(a) MCM current control operation at power factor of 0.95

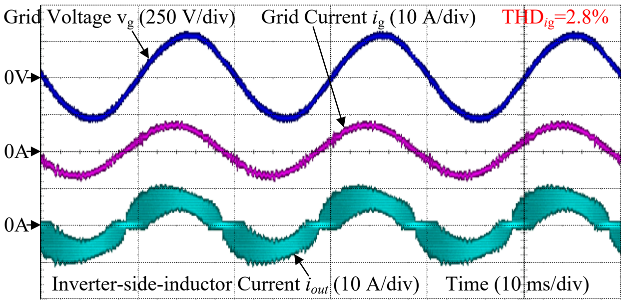

(b) MCM current control operation at power factor of 0.90

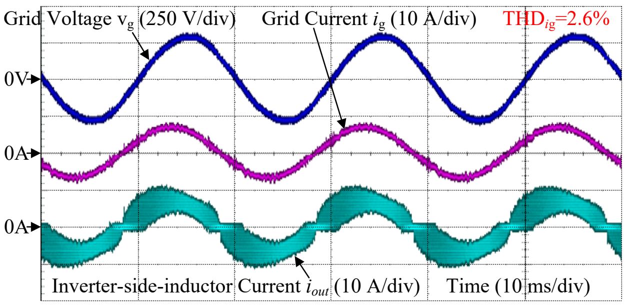

(c) MCM current control operation at power factor of 0.85

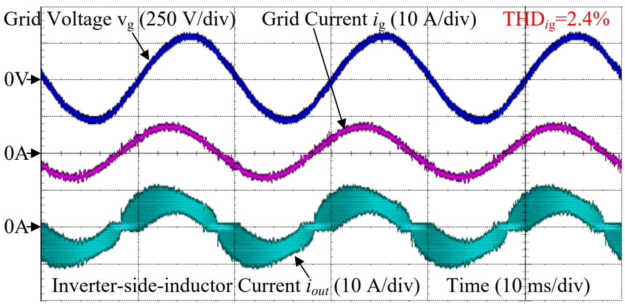

(d) MCM current control operation at power factor of 0.80

Fig. 15. Proposed MCM current control operation at rated current and under different power factors. The low grid current THD can still be achieved at low power factor with the proposed MCM current control. On the other words, the proposed MCM current control provides the grid-tied inverter the capability of fault-ride-through.

linearity occurs in the disturbance response which leads to the natural decrease in the disturbance gain at light load. By utilizing this DCM nonlinearity in the disturbance response, the grid current THD is maintained below 5% over entire load range even with the small normalized impedance of the grid-side inductor of 0.16%.

The main contribution of this paper is that the proposed MCM current control is independent from the inductor value because the inductor value is not used in both the DCM nonlinearity compensation and the current mode determination.

REFERENCES

[1] R. Chattopadhyay, S. Bhattacharya, N. C. Foureaux, I. A. Pires, H. de Paula, L. Moraes, P. C. Cortizio, S. M. Silva, B. C. Filho, J. A. de S. Brito, "Low-Voltage PV Power Integration into Medium Voltage Grid Using High-Voltage SiC Devices," *IEEJ J. Ind. Appl.*, vol. 4, no. 6, pp.767-775, Nov. 2015.

[2] D. Bortis, D. Neumayr, J. W. Kolar, "ηρ-Pareto Optimization and Comparative Evaluation of Inverter Concepts considered for the GOOGLE Little Box Challenge", Proceedings of the 17th IEEE Workshop on Control and Modeling for Power Electronics (COMPEL 2016), Trondheim, Norway, June 27-30, 2016.

[3] Y. Lei *et al.*, "A 2-kW Single-Phase Seven-Level Flying Capacitor Multilevel Inverter With an Active Energy Buffer," in *IEEE Transactions on Power Electronics*, vol. 32, no. 11, pp. 8570-8581, Nov. 2017.

[4] M. Liserre, F. Blaabjerg, and S. Hansen, "Design and Control of an LCL-Filter-Based Three-Phase Active Rectifier," *IEEE Trans. Power Electron.*, vol. 41, no. 5, pp. 1281-1291, Nov. 2005.

[5] A. Reznik, M. G. Simões, A. Al-Durra, S. M. Muyeen, "LCL Filter Design and Performance Analysis for Grid-Interconnected Systems," *IEEE Trans. Ind. Appl.*, vol. 50, no. 2, pp. 1225-1232, Apr. 2014.

[6] J. Imaoka, K. Umetani, S. Kimura, W. Martinez, M. Yamamoto, S. Arimura, T. Hirano, "Magnetic Analysis, Design, and Experimental Evaluations of Integrated Winding Coupled Inductors in Interleaved Converters," *IEEJ J. Ind. Appl.*, vol. 5, no. 3, pp. 276–288, May 2016.

[7] K. Senda, H. Toda, M. Kawano, "Influence of Interlocking on Core Magnetic Properties," *IEEJ J. Ind. Appl.*, vol. 4, no. 4, pp.496-502, Jul. 2015.

[8] S. Nagai, Hoai Nam Le, T. Nagano, K. Orikawa and J. i. Itoh, "Minimization of interconnected inductor for single-phase inverter with high-performance disturbance observer," *2016 IEEE 8th International Power Electronics and Motion Control Conference (IPEMC-ECCE Asia)*, Hefei, 2016, pp. 3218-3225.

[9] J. Sun, D. M. Mitchell, M. F. Greuel, Ph. T. Krein, R. M. Bass, "Averaged Modeling of PWM Converters Operating in Discontinuous Conduction Mode," *IEEE Trans. Power Electron.*, vol. 16, no. 4, pp. 482-492, Jul. 2001.

[10] H. N. Le, K. Orikawa, J. Itoh, "Circuit-Parameter-Independent Nonlinearity Compensation for Boost Converter Operated in Discontinuous Current Mode," *IEEE Trans. Ind. Electron.*, vol. 64, no. 2, pp. 1157-1166, Feb. 2017.

[11] K. D. Gusseme, D. M. V. de Sype, A. P. V. den Bossche, and J. A. Melkebeek, "Digitally Controlled Boost Power-Factor-Correction Converters Operating in Both Continuous and Discontinuous Conduction Mode," *IEEE Trans. Power Electron.*, vol. 52, no. 1, pp. 88-97, Feb. 2005.

[12] Sh. F. Lim, and A. M. Khambadkone, "A Simple Digital DCM Control Scheme for Boost PFC Operating in Both CCM and DCM," *IEEE Trans. Power Electron.*, vol. 47, no. 4, pp. 1802-1812, Aug. 2011.

[13] T. S Hwang, and S. Y. Park, "Seamless Boost Converter Control Under the Critical Boundary Condition for a Fuel Cell Power Conditioning System," *IEEE Trans. Power Electron.*, vol. 27, no. 8, pp. 3616-3626, Aug. 2012.

[14] C. W. Clark, F. Musavi, and W. Eberle, "Digital DCM Detection and Mixed Conduction Mode Control for Boost PFC Converters," *IEEE Trans. Power Electron.*, vol. 29, no. 1, pp. 347-355, Jan. 2014.

[15] B. A. Ferrari, N. R. N. Ama, K. C. M. Carvalho, F. O. Martinz, and L. M. Junior, "Robust Control Design for Voltage Tracking Loop of Dynamic Voltage Restorers," *IEEJ J. Ind. Appl.*, vol. 4, no. 5, pp. 634-642, Sep. 2015.